

ARMY RESEARCH LABORATORY



Progress Toward a Multidimensional Representation of Mortar Interior Ballistics

by John R. Schmidt and Michael J. Nusca

ARL-TR-4839

June 2009

NOTICES

Disclaimers

The findings in this report are not to be construed as an official Department of the Army position unless so designated by other authorized documents.

Citation of manufacturer's or trade names does not constitute an official endorsement or approval of the use thereof.

Destroy this report when it is no longer needed. Do not return it to the originator.

Army Research Laboratory

Aberdeen Proving Ground, MD 21005-5066

ARL-TR-4839

June 2009

Progress Toward a Multidimensional Representation of Mortar Interior Ballistics

**John R. Schmidt and Michael J. Nusca
Weapons and Materials Research Directorate, ARL**

| REPORT DOCUMENTATION PAGE | | | Form Approved OMB No. 0704-0188 | | |
|---|------------------------------------|-------------------------------------|--|--|--|
| Public reporting burden for this collection of information is estimated to average 1 hour per response, including the time for reviewing instructions, searching existing data sources, gathering and maintaining the data needed, and completing and reviewing the collection information. Send comments regarding this burden estimate or any other aspect of this collection of information, including suggestions for reducing the burden, to Department of Defense, Washington Headquarters Services, Directorate for Information Operations and Reports (0704-0188), 1215 Jefferson Davis Highway, Suite 1204, Arlington, VA 22202-4302. Respondents should be aware that notwithstanding any other provision of law, no person shall be subject to any penalty for failing to comply with a collection of information if it does not display a currently valid OMB control number. PLEASE DO NOT RETURN YOUR FORM TO THE ABOVE ADDRESS. | | | | | |
| 1. REPORT DATE (DD-MM-YYYY) June 2009 | | 2. REPORT TYPE Final | | 3. DATES COVERED (From - To) May 2007–March 2008 | |
| 4. TITLE AND SUBTITLE Progress Toward a Multidimensional Representation of Mortar Interior Ballistics | | | 5a. CONTRACT NUMBER | | |
| | | | 5b. GRANT NUMBER | | |
| | | | 5c. PROGRAM ELEMENT NUMBER | | |
| 6. AUTHOR(S) John R. Schmidt and Michael J. Nusca | | | 5d. PROJECT NUMBER 622618H8000 | | |
| | | | 5e. TASK NUMBER | | |
| | | | 5f. WORK UNIT NUMBER | | |
| 7. PERFORMING ORGANIZATION NAME(S) AND ADDRESS(ES) U.S. Army Research Laboratory ATTN: AMSRD-ARL-WM-BD Aberdeen Proving Ground, MD 21005-5066 | | | 8. PERFORMING ORGANIZATION REPORT NUMBER ARL-TR-4839 | | |
| 9. SPONSORING/MONITORING AGENCY NAME(S) AND ADDRESS(ES) | | | 10. SPONSOR/MONITOR'S ACRONYM(S) | | |
| | | | 11. SPONSOR/MONITOR'S REPORT NUMBER(S) | | |
| 12. DISTRIBUTION/AVAILABILITY STATEMENT Approved for public release; distribution is unlimited. | | | | | |
| 13. SUPPLEMENTARY NOTES | | | | | |
| 14. ABSTRACT Lumped-parameter interior ballistics (IB) codes have had limited success in simulating the IB of mortars due to the complex nature of the firing event. Only near the end of the firing event does the mortar conform to the conventional ballistics model for which lumped-parameter codes were designed. Modified lumped-parameter models are capable of simulating some key mortar variables. There are significant pressure waves developed in mortars, which are due in part to the nonuniform discharge of combustion products from the flashtube. The mortar IB cycle is not only time dependant but is also very spatially complex. These pressure waves cannot be adequately represented in a one-dimensional IB model. Plans to modify the Army's two- or three-dimensional IB code ARL-NGEN3 for mortar simulations are discussed. However, conventional NGEN modeling approaches cannot capture the nonuniform discharge of combustion products from the flashtube as shown in experiments. An improvement in gas generation tables and work on a two-phase turbulence model of a primer and black powder pellets with a velocity profile based on the one-dimensional turbulence modeling approach are presented. Plans for coupling this primer model to the ARL-NGEN3 code for mortars are discussed. | | | | | |
| 15. SUBJECT TERMS interior ballistics, primer, CFD, two-phase flow, guns, mortars | | | | | |
| 16. SECURITY CLASSIFICATION OF: | | | 17. LIMITATION OF ABSTRACT UU | 18. NUMBER OF PAGES 38 | 19a. NAME OF RESPONSIBLE PERSON John R. Schmidt |
| a. REPORT Unclassified | b. ABSTRACT Unclassified | c. THIS PAGE Unclassified | | | 19b. TELEPHONE NUMBER (Include area code) 410-278-5510 |

Contents

| | |
|--|-----------|
| List of Figures | iv |
| Acknowledgments | vi |
| 1. Background | 1 |
| 2. Modeling Using the ARL-NGEN3 Code | 2 |
| 2.1 Results for an Assumed Igniter Table | 3 |
| 2.2 Results for a Detailed Igniter Table | 11 |
| 3. Dedicated Igniter Submodel | 19 |
| 4. Conclusions | 22 |
| 5. References | 23 |
| Distribution List | 25 |

List of Figures

| | |
|--|----|
| Figure 1. Schematic of a mortar system: (a) footplate and tube, (b) projectile in tube, and (c) cross section of tail boom. | 1 |
| Figure 2. ARL-NGEN3 code setup for mortar simulation (see text for identification of numbered regions). | 4 |
| Figure 3. ARL-NGEN3 code results for tube wall pressures at three axial locations (see figure 2). | 4 |
| Figure 4. ARL-NGEN3 code results for contours of charge boundaries, propellant temperature, and gas pressure with selected velocity vectors. Time since igniter function is 0.2 ms. | 6 |
| Figure 5. ARL-NGEN3 code results for contours of charge boundaries, propellant temperature, and gas pressure with selected velocity vectors. Time since igniter function is 0.4 ms. | 6 |
| Figure 6. ARL-NGEN3 code results for contours of charge boundaries, propellant temperature, and gas pressure with selected velocity vectors. Time since igniter function is 0.6 ms. | 7 |
| Figure 7. ARL-NGEN3 code results for contours of charge boundaries, propellant temperature, and gas pressure with selected velocity vectors. Time since igniter function is 1.0 ms. | 7 |
| Figure 8. ARL-NGEN3 code results for contours of charge boundaries, propellant temperature, and gas pressure with selected velocity vectors. Time since igniter function is 1.05 ms. | 8 |
| Figure 9. ARL-NGEN3 code results for contours of charge boundaries, propellant temperature, and gas pressure with selected velocity vectors. Time since igniter function is 1.35 ms. | 8 |
| Figure 10. ARL-NGEN3 code results for contours of charge boundaries, propellant temperature, and gas pressure with selected velocity vectors. Time since igniter function is 2.25 ms. | 9 |
| Figure 11. ARL-NGEN3 code results for contours of charge boundaries, propellant temperature, and gas pressure with selected velocity vectors. Time since igniter function is 2.7 ms. | 9 |
| Figure 12. ARL-NGEN3 code setup for mortar simulation (see text for identification of numbered regions). | 11 |
| Figure 13. ARL-NGEN3 code results for tube wall pressures at three axial locations (see figure 12). | 12 |
| Figure 14. ARL-NGEN3 code results for contours of charge boundaries, propellant temperature, and gas pressure with selected velocity vectors. Time since igniter function is 1.35 ms. | 13 |

| | |
|---|----|
| Figure 15. ARL-NGEN3 code results for contours of charge boundaries, propellant temperature, and gas pressure with selected velocity vectors. Time since igniter function is 1.6 ms..... | 13 |
| Figure 16. ARL-NGEN3 code results for contours of charge boundaries, propellant temperature, and gas pressure with selected velocity vectors. Time since igniter function is 1.75 ms..... | 14 |
| Figure 17. ARL-NGEN3 code results for contours of charge boundaries, propellant temperature, and gas pressure with selected velocity vectors. Time since igniter function is 2.0 ms..... | 14 |
| Figure 18. ARL-NGEN3 code results for contours of charge boundaries, propellant temperature, and gas pressure with selected velocity vectors. Time since igniter function is 2.4 ms..... | 15 |
| Figure 19. ARL-NGEN3 code results for contours of charge boundaries, propellant temperature, and gas pressure with selected velocity vectors. Time since igniter function is 2.45 ms..... | 15 |
| Figure 20. ARL-NGEN3 code results for contours of charge boundaries, propellant temperature, and gas pressure with selected velocity vectors. Time since igniter function is 2.75 ms..... | 16 |
| Figure 21. ARL-NGEN3 code results for contours of charge boundaries, propellant temperature, and gas pressure with selected velocity vectors. Time since igniter function is 3.6 ms..... | 16 |
| Figure 22. ARL-NGEN3 code results for contours of charge boundaries, propellant temperature, and gas pressure with selected velocity vectors. Time since igniter function is 4.05 ms..... | 17 |

Acknowledgments

Mr. Albert Horst (U.S. Army Research Laboratory [ARL] contractor) is acknowledged for his efforts in assembling an initial set of mortar system ballistics data and preparing the corresponding ballistics code input files. Mr. Horst conducted a detailed study of the mortar igniter data generated at Penn State University (PSU), interpreted the PSU data in order to deduce mass flow rates, and generated both simple and detailed tables for inclusion into the ARL-NGEN code.

1. Background

The modern smoothbore U.S. Army mortar (figure 1) is basically a gun tube with a firing pin fixed to the breech end. The mortar round is muzzle loaded, gravity fed, and completely self-contained with a payload, primer, booster charge of black powder (BP), an igniter charge contained in a high-pressure canister within the tail boom, and the option of up to four modules of primary propellant bags installed around the tail boom. The modules can be removed in order to achieve the desired muzzle velocity which, in turn, determines the distance traveled by the mortar round. Mortars are fired at very steep angles. Once in flight, most modern mortar rounds are fin stabilized; however, there are some mortar rounds which are spin stabilized. The original designs are reminiscent of the apothecary mixing vessels after which they were named. Mortars have short barrel lengths compared to their diameters, usually <math><20</math> cal. long. Maneuverable mortars were first used in battle in the late seventeenth century.

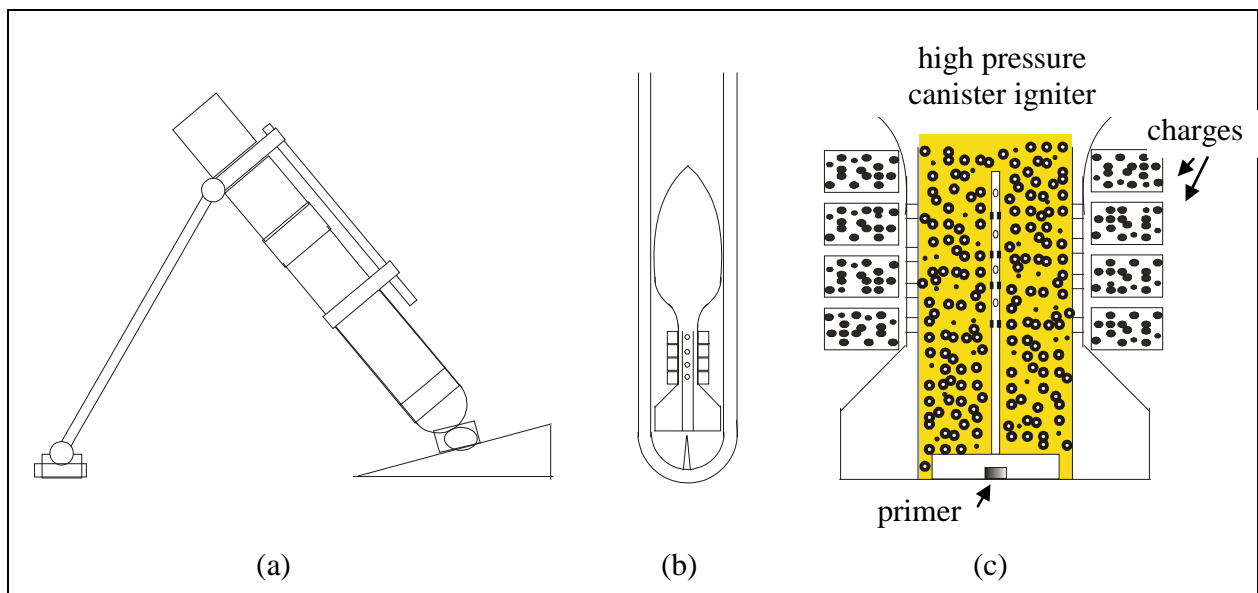


Figure 1. Schematic of a mortar system: (a) footplate and tube, (b) projectile in tube, and (c) cross section of tail boom.

Mortars by their very nature are useful in ground maneuvers; history has shown their effectiveness in battles against defilade (dug-in) enemy troops and targets not easily defeated by direct-fire weapons. This effectiveness is due to the high angle of attack of mortar weapons. Though not very successful against bunkers or tanks, mortars achieved great acclaim during the trench warfare of World War I when a highly mobile type called a “Stokes Mortar” was

developed. Mortars provide accurate close-in fire for ground troops during battle without the overhead necessary for artillery pieces. Mortar rounds are generally of three battle types—high explosive, illuminating, and smoke producing. A plethora of practice rounds is used for training. “Smart” mortar rounds have been in production since 1994, and the U.S. Army is developing a precision-guided mortar munition. The U.S. Army has a vested interest in understanding the science involved in the firing of mortar rounds, with the objective of leveraging this knowledge for improved interior ballistics (IB) models. The long-range goal is improved design and function of the mortar rounds, yielding better accuracy and precision.

In the past, lumped-parameter IB codes such as IBHVG2 (1) have had limited success in simulating mortars due to the complex nature of the firing event. Initiation of the percussion primer ignites the booster charge of BP pellets. The efflux of the burning BP exits the perforated flashtube where it ignites and initiates flame spreading of the main propelling charge in the tail boom. After a sufficient pressure is built up inside the tail boom, hot gasses and burning particles are discharged into the mortar tube, which may or may not have additional propellant modules. Finally, the mortar tube with burning propellant and hot expanding gasses conforms to the conventional ballistics model for which lumped-parameter codes were designed. However, as Kuo et al. (2) point out, there are significant pressure waves developed in a mortar, which are due, in part, to the nonuniform discharge of combustion products from the flashtube. May and Horst (3) demonstrate the complexities involved in attempting to eliminate the occurrence of pressure waves.

Recent additions to the IBHVG2 code (1) allow the modeling of two chambers to represent the mortar configuration. There is a high-pressure canister representing the tail boom and a low-pressure chamber representing the mortar tube exterior to the tail boom. This high-low (HILO) feature has proved useful to the lumped-parameter IB modeling of mortars. Schmidt et al. (4) discuss using HILO and its application to a notional U.S. Army mortar round using the new feature to generate sensitivity curves. The mortar IB cycle is not only time dependant but very spatially complex, some features of which are clearly outside the purview of a one-dimensional (1-D) IB model. All these considerations underpin the need for a multidimensional representation containing the relevant physics.

2. Modeling Using the ARL-NGEN3 Code

Since one of the primary motivations for the present work is to develop a primer model compatible with the ARL-NGEN3 IB code, a brief description of this code is included for completeness. For further details, the reader is referred to papers by Gough (5, 6) and Nusca and coworkers (7–12) for a review of the governing equations and selected code applications.

The Army's NGEN3 code is a multidimensional, multiphase computational fluid dynamics code that incorporates three-dimensional (3-D) continuum equations along with auxiliary relations into a modular code structure. On a sufficiently small scale of resolution in space and time, the components of the IB flow are represented by the balance equations for a multicomponent reacting mixture describing the conservation of mass, momentum, and energy. A macroscopic representation of the flow is adopted using these equations derived by a formal averaging technique applied to the microscopic flow. These equations require a number of constitutive laws for closure, including state equations, intergranular stresses, and interphase transfer. The numerical representation of these equations, as well as the numerical solution thereof, is based on a finite-volume discretization and high-order, accurate, conservative numerical solution schemes. The spatial values of the dependent variables at each time step are determined by a numerical integration method, denoted the continuum flow solver (CFS), treating the continuous phase and certain discrete phases in Eulerian fashion.

The flux-corrected transport scheme is a suitable basis for the CFS since the method is numerically explicit, computationally robust, and has been shown to adapt easily to massively parallel computer systems. The discrete phases are treated by a Lagrangian formulation, denoted the large particle integrator (LPI), tracking the particles explicitly and smoothing discontinuities associated with boundaries between propellants and yielding a continuous distribution of porosity over the entire domain. The manner of coupling between the CFS and the LPI is through the attribution of properties (e.g., porosity and mass generation). The size of the grid, as well as the number of Lagrangian particles, is user prescribed. The solid propellant is modeled using Lagrange particles that regress, produce combustion product gases, and respond to gas-dynamic and physical forces. Individual grains, balls, sticks, slabs, and wrap layers are not resolved; rather, each propellant medium is distributed within a specified region in the gun chamber. The constitutive laws that describe interphase drag, form-function, etc., assigned to these various media determine preferred gas flow paths through the media (e.g., radial for disks and axial for wraps) and responses of the media to gas-dynamic forces. Media regions that are encased in impermeable boundaries, which only yield to gas-dynamic flow after a prescribed pressure load is reached, act as rigid bodies within the chamber. Using computational particles to represent the propellant charge permits a host of modeling features that enhances the representation of charge details.

2.1 Results for an Assumed Igniter Table

Figure 2 shows a schematic of the computational domain used in the ARL-NGEN3 code for the current simulation of the 120-mm mortar. (Note that figure 2 has the ordinate magnified by approximately a factor of 7.) In the axial direction, the domain extends from the breech face ($X = 0$) to the base of the projectile at 47 cm (i.e., defined for the present application as the location on the projectile where the diameter matches that of the launch tube). Since an axisymmetric configuration is assumed, the domain extends in the radial direction from the centerline to the radial wall of the mortar tube (6-cm radius), and the fin set is excluded. For the

ARL-NGEN3 code, the tail boom of the mortar (i.e., the region extending axially from the tube breach to 21 cm, with a radius of 2.1 cm), while joined to the afterbody of the mortar, is nonetheless modeled as part of the overall propelling charge and ignition mechanism, with explicit treatment of the internal tail boom components. The black, green, and purple “dots” located on the radial tube wall mark the location at which wall pressure values are collected as a function of time (see discussions for figure 3).

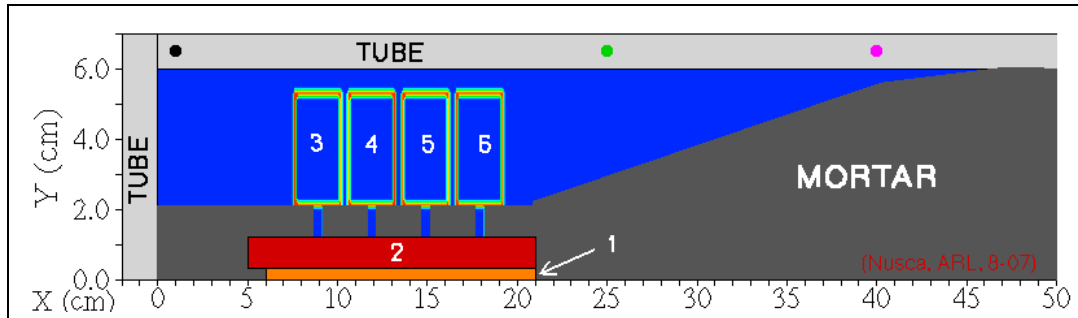


Figure 2. ARL-NGEN3 code setup for mortar simulation (see text for identification of numbered regions).

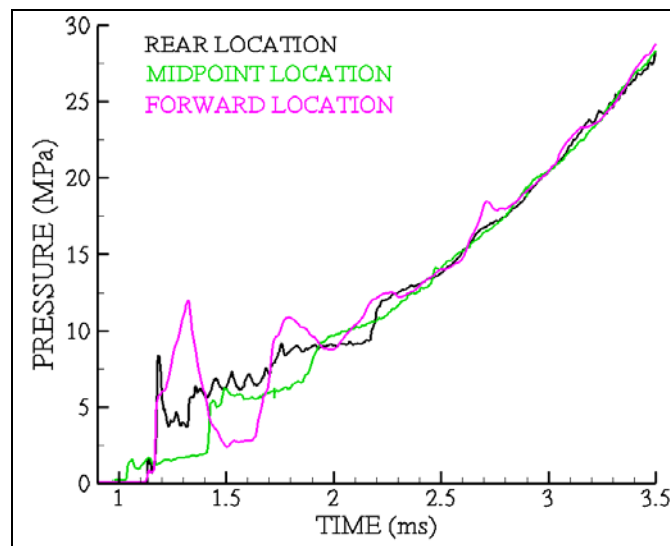


Figure 3. ARL-NGEN3 code results for tube wall pressures at three axial locations (see figure 2).

Several regions of charge and/or ignition stimuli are identified in the figure. Region 1 extends along the centerline from 6 to 21 cm within the tail boom and represents the innermost tube of the igniter (radius of 0.32 cm). In the actual mortar, this region is empty, while the primer and five pellets of BP are housed behind region 1 (i.e., rear of 6 cm). An array of radial holes vents primer, burning BP, and other gases into region 2. In the model, region 1 is occupied by an igniter mass-flow table that essentially generates an even spatial distribution of hot gases from BP (1 g) that is fully ignited at time 0 and burns for 2 ms. In the next section of this report, an

improvement of the representation for region 1 is detailed. Region 2 is occupied with 60 g of M48 (undeterred ball propellant), which is distributed along the length of the inner tube from 5 to 21 cm and extends radially from 0.32 to 1.2 cm (i.e., diameter of 2.4 cm around the inner tube of 0.64 cm). This region of propellant is directly exposed to region 1; there is no consideration of a physical radial barrier between regions 1 and 2. The inclusion of this detail is delayed to future work but is within the present capability of the model. Regions 3–6 are four axisymmetric charges, each containing 115 g of M47 propellant. The M47 is a deterred ball propellant consisting of a core and a surface coating, each of which has distinct burn rate properties in this model. The diameter of the M47 propellant grain is about half that of the M48 propellant. Region 2 is separated from the axisymmetric charges (regions 3–6) by a solid section of the tailboom perforated with four radial strips at the outer radius (2.1 cm) and beneath each of the four charges. We note that, in practice, these radial strips are actually an array of holes, the inclusion of which would require a fully 3-D modeling treatment. In addition, the charges (regions 3–6) are not cylindrical but actually “horseshoe-shaped,” which also requires a 3-D treatment. While these 3-D details are within the capability of the model, treatment of these is being reserved for future work.

The ARL-NGEN3 code models each of these regions (i.e., 2–6) of ball propellant explicitly using an array of Lagrange particles that are initially arranged within the boundaries of each region but are free to move according to the appropriate governing equations as the simulation proceeds. Each LPI particle then carries the same physical and thermodynamic properties as the individual grains in its immediate vicinity using a number weighting factor. The walls of the tail boom (depicted in figure 2 as enclosing regions 1 and 2) are solid regions in the model and managed by internal boundary condition routines. The walls of each charge module (i.e., regions 3–6) are composed of combustible case material (with an energy of about 2300 J/g), with distinct thermodynamic, mass, and burning parameters. These walls are represented by special Lagrange particles, which remain impermeable (hence the charges act as rigid bodies) until a specified wall overpressure is reached or a wall burn-through condition is realized.

Yielding of the charge walls is spatially resolved in the model. Nominal overpressure burst criterion was utilized; however, there is a future requirement for a modeling sensitivity study involving this parameter.

Computed wall pressures as a function of time for three locations along the tube wall (see figure 2) are displayed in figure 3. This figure can be used as a guide to the subsequent discussion of detailed modeling results displayed in figures 4–11. (Note that figures 4–11 have the ordinate magnified by approximately a factor of 7.) Prior to about 1 ms, propellant burning is confined to the tailboom, as evidenced by the nonexistent pressurization of the launch tube before this time. Early time pressure transients from about 1.05 to 1.35 ms indicate the bursting of the propellant increments. Pressure waves traveling between the rear and forward pressure taps are clearly evidenced by the alternating pressure peaks and troughs most readily seen from about 1.4 to 2.5 ms. The launch tube is then evenly pressurized, leading to projectile movement after about 3.5 ms.

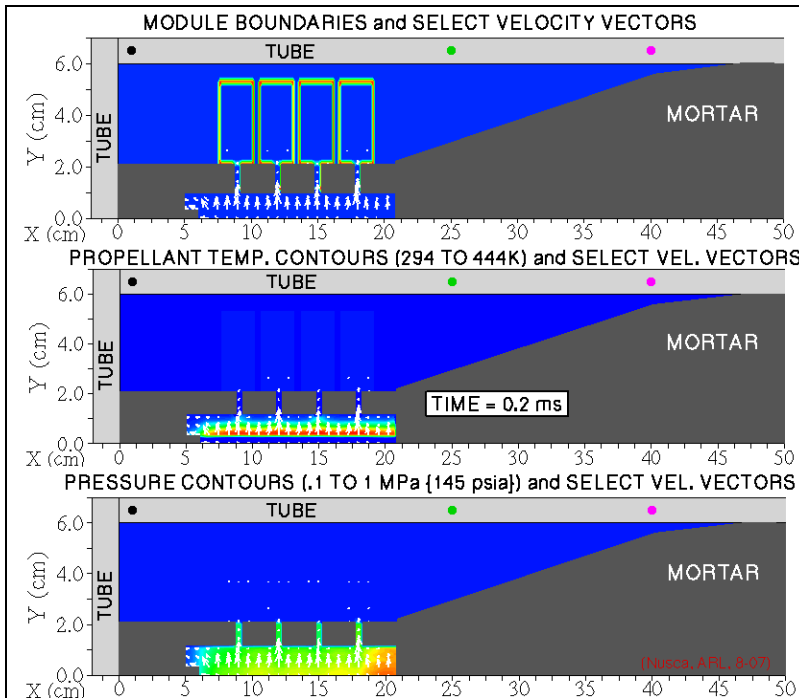


Figure 4. ARL-NGEN3 code results for contours of charge boundaries, propellant temperature, and gas pressure with selected velocity vectors. Time since igniter function is 0.2 ms.

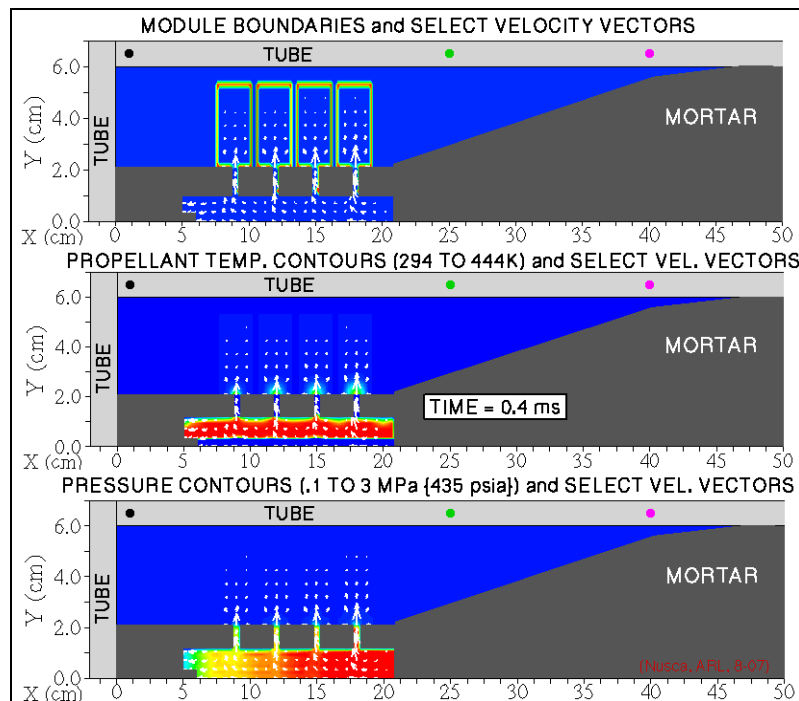


Figure 5. ARL-NGEN3 code results for contours of charge boundaries, propellant temperature, and gas pressure with selected velocity vectors. Time since igniter function is 0.4 ms.

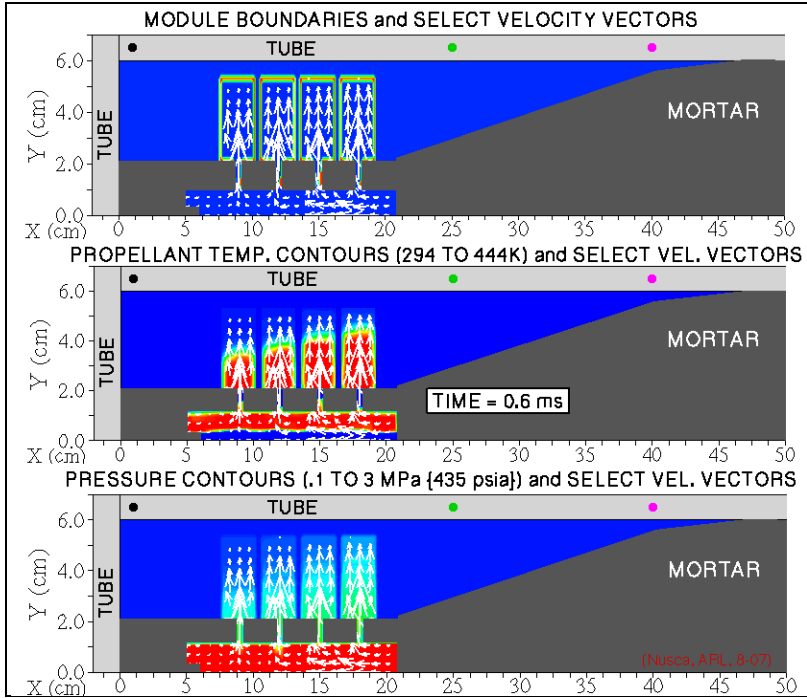


Figure 6. ARL-NGEN3 code results for contours of charge boundaries, propellant temperature, and gas pressure with selected velocity vectors. Time since igniter function is 0.6 ms.

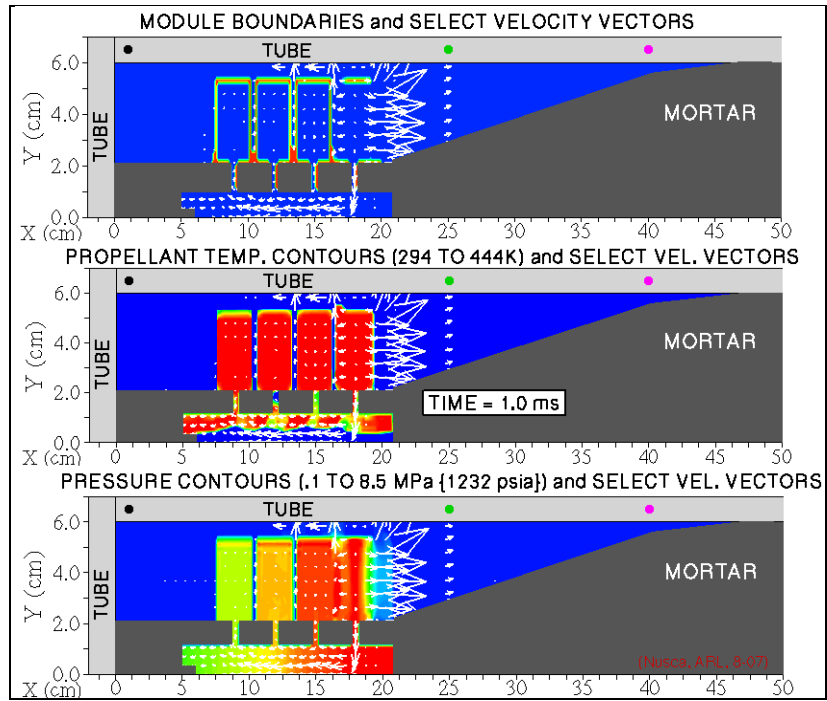


Figure 7. ARL-NGEN3 code results for contours of charge boundaries, propellant temperature, and gas pressure with selected velocity vectors. Time since igniter function is 1.0 ms.

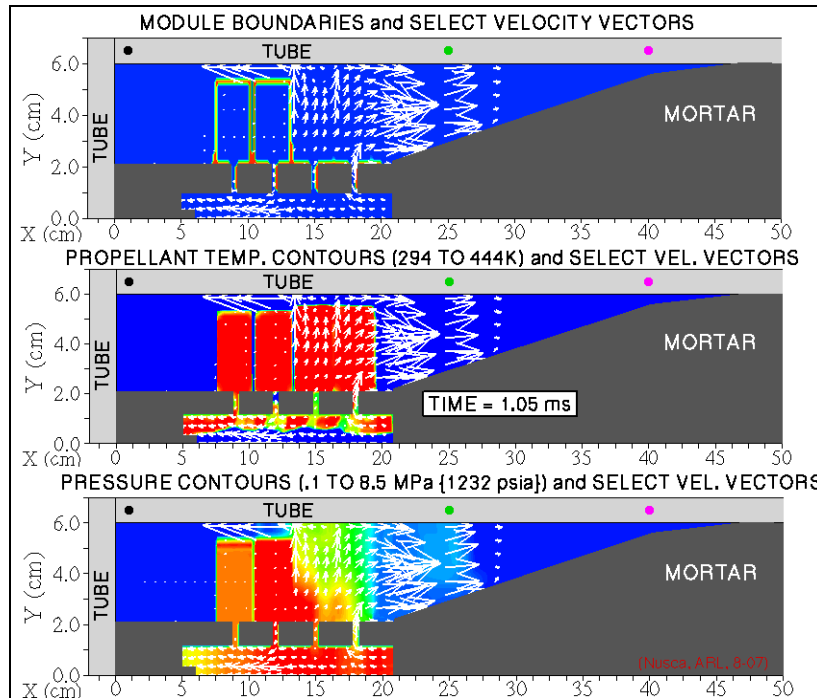


Figure 8. ARL-NGEN3 code results for contours of charge boundaries, propellant temperature, and gas pressure with selected velocity vectors. Time since igniter function is 1.05 ms.

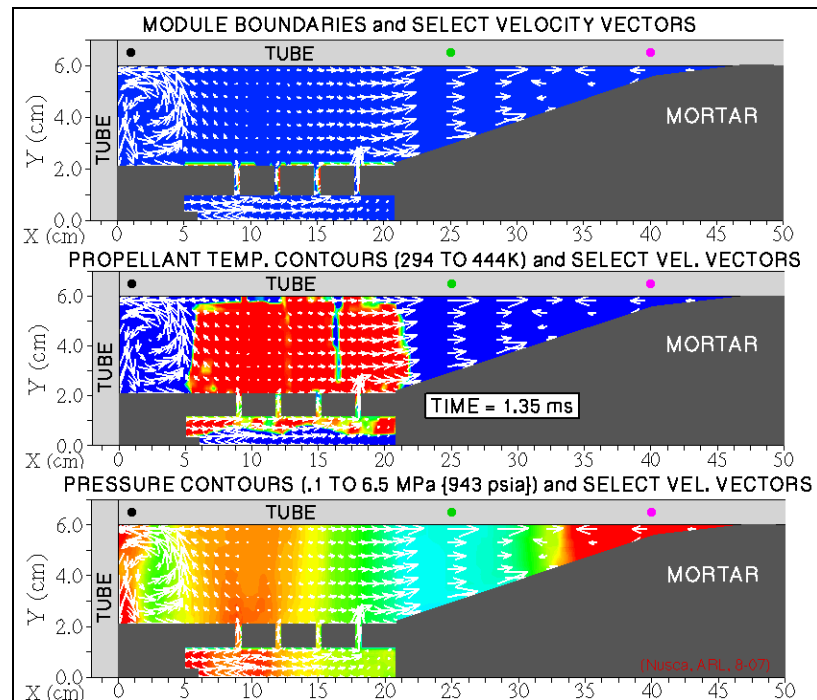


Figure 9. ARL-NGEN3 code results for contours of charge boundaries, propellant temperature, and gas pressure with selected velocity vectors. Time since igniter function is 1.35 ms.

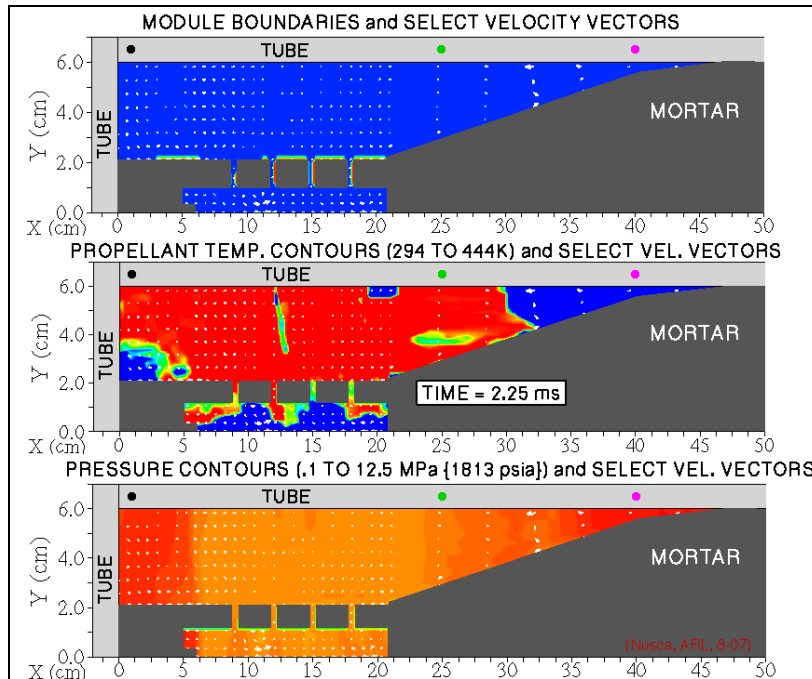


Figure 10. ARL-NGEN3 code results for contours of charge boundaries, propellant temperature, and gas pressure with selected velocity vectors. Time since igniter function is 2.25 ms.

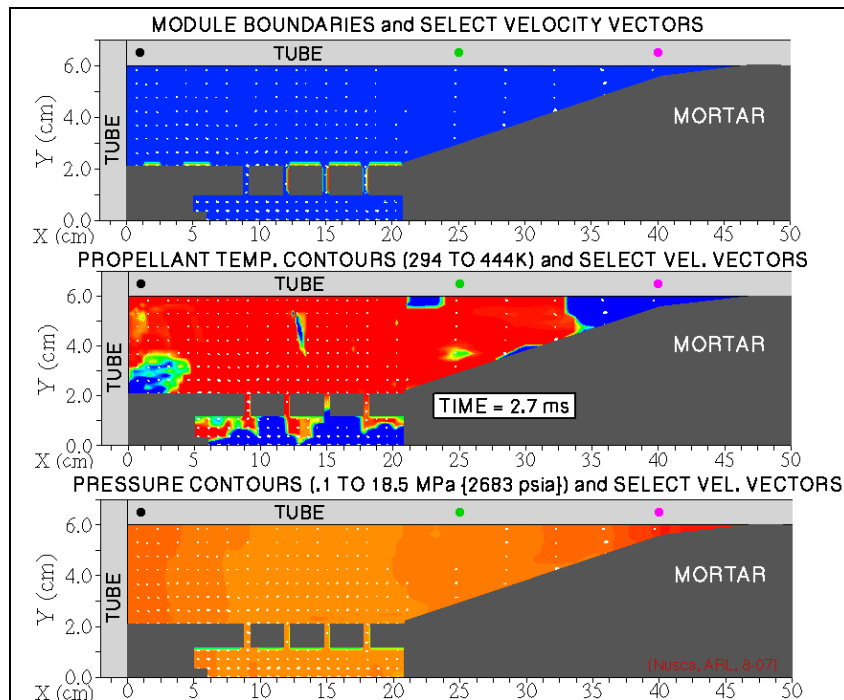


Figure 11. ARL-NGEN3 code results for contours of charge boundaries, propellant temperature, and gas pressure with selected velocity vectors. Time since igniter function is 2.7 ms.

The detailed results of the ARL-NGEN3 simulation are displayed in figures 4–11 for times of 0.2–2.7 ms from the start of outflow from region 1 (see figure 2). During this time period, the ignition and flame spreading are prominent. After 2.7 ms, the mortar begins to travel down the tube (modeling results are not presented for times greater than 2.7 ms for brevity). In each figure, a particular time is displayed using three computed variables—module boundaries, propellant temperature, and gas pressure. Velocity vectors (in white) are overlaid in each case to display the magnitude (via length) and direction of the local gas field. Module boundaries are red when solid (red to light green due to graphical rendering) and change color to indicate loss in integrity due to a combination of burn-through and burst due to overpressure. When a charge module has fully disintegrated, module boundaries are no longer displayed. The location of ignited propellant is indicated by colors from green to red (i.e., warm temperature to ignition temperature). High gas pressure is indicated by red, with lower pressures indicated by a succession of colors from orange to blue.

Figure 4 shows results just past the start of the simulation. Burning BP within the inner igniter region produces gases that flow radially and begin ignition of the M48 propellant within the tailboom. Gases begin to flow into the annular slots, and flow stagnation to about 1 MPa is observed in the igniter. By 0.4 ms (figure 5), the M48 propellant is fully ignited, and pressurization of the enclosed tailboom is ~3 MPa. Even though the increments are still intact, high-pressure flow through the annular slots in the tailboom has begun to penetrate the four propellant modules external to the tailboom. By 0.6 ms (figure 6), high-velocity gas flow through the annular slots and into the increments has caused ignition of the M47 propellant, even though the propellant modules are still intact. As expected, the right-most increment (i.e., region 6) shows advanced flame spreading due to the higher pressure (stagnated) gas in the forward end of the tailboom. Subsequently, by 1.0 ms (figure 7), the fourth increment bursts due to overpressures exceeding 8.5 MPa. Support from the third increment causes the burst of the fourth increment to occur in the forward direction.

In response to the burst event, the rearward movement of the remaining intact increments has closed the interincrement gaps. It is interesting to note the gas flow is now forced back down through the fourth annular slot and into the tailboom, raising the internal pressure to about 8.5 MPa, while M48 propellant within the tailboom is forced up through the first and second annular slots. By 1.05 ms (figure 8), another increment yields, and by 1.35 ms (figure 9), all of the increments have burst, and M47 propellant is free to move in the launch tube, whereas high pressure in the launch tube had been confined to the region near the propellant increments. After 1.35 ms (figure 9), uneven pressurization of the entire launch tube behind the mortar is observed as well as several two-dimensional (2-D) flow phenomena (e.g., vortices). One can also observe high-velocity gas flow onto the mortar afterbody and returning to the rear of the launch tube. These pressure waves are the source of discontinuous forces and stresses on the mortar prior to launch. Between 2.25 and 2.7 ms (figures 10 and 11), unconfined M47 propellant is spreading throughout the launch tube as, essentially, even pressurization of the chamber to levels exceeding 18 MPa is occurring. After these events, the projectile begins forward motion up the launch tube.

The next step in improving the fidelity and detail of the modeling of the mortar launch is to include an approach to the representation of the centercore ignition stimulus based on actual measurements of the outflow from the center tube igniter (i.e., region 1 of figure 2). The next section deals with such a simulation.

2.2 Results for a Detailed Igniter Table

Figure 12 shows a schematic of the computational domain used in the ARL-NGEN3 code for the current simulation of the 120-mm mortar. (Note that figure 12 has the ordinate magnified by about a factor of 7.) This schematic is nearly identical to the one shown in figure 2 and discussed in the last section. The sole difference here is that the axial extent of region 1 has been changed to extend from 8.3 to 18.64 cm (radius 0.32 cm). Region 1's axial dimension was chosen to coincide with the approximate length covered by a series of holes designed to vent gases from the center tube (region 1) to region 2 (see discussion following). The other regions identified in the figure are identical to those discussed in reference to figure 2 in the last section of this report.

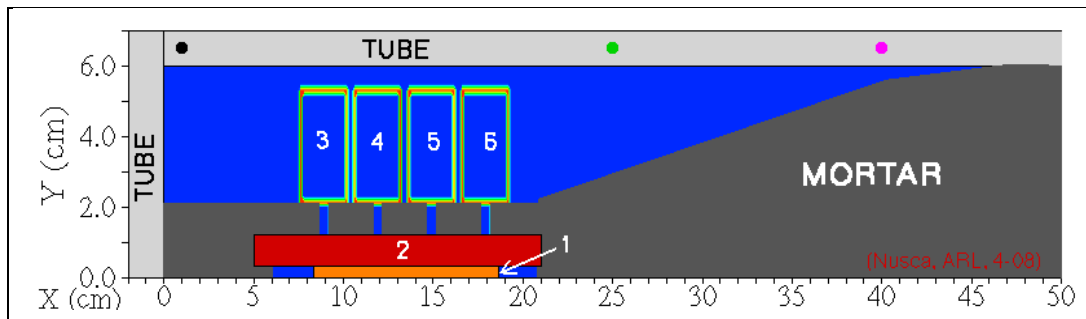


Figure 12. ARL-NGEN3 code setup for mortar simulation (see text for identification of numbered regions).

At this stage, a more detailed and perhaps more accurate representation of the mass output from the mortar igniter during the ignition phase is required for linkage to the ARL-NGEN3 code. A detailed igniter table representing the mass output (i.e., mass per unit volume and per unit time) for region 1 (figure 12) was generated using the experimental data produced by Kuo et al. (2). In the experimental study, the mortar flash tube was instrumented using pressure taps near five representative vent holes of the 20 actual holes. Kuo et al. (2) computed the assumed temporal mass flow rate along the tube using these discrete pressure data. The detailed igniter table for the ARL-NGEN3 code was assembled using these data; five cylindrical regions, internal to the flashtube, were chosen to encompass the axial extent of the vent holes along the tube. The volumes of these five regions were assumed to be the same volume into which the combustion products of the flashtube material (black powder pellets) were discharged during the ignition event. Additional vent holes that resided within each of the five regions but were not assigned corresponding pressure taps during the test were assumed to exhibit similar pressure/time

behavior as neighboring measurement stations. Twenty time increments were used to probe the test data, leading to a table of flashtube output (i.e., mass addition into the assigned subregions of region 1, figure 2) for 10 axial stations of 2 radial stations each and at 40× during the ignition interval. Validation of this detailed tabular representation was accomplished by numerically evaluating and then summing mass flux from each regional volume and for each time increment, yielding a total consumption of about 67% of the initial mass of the five black powder pellets in the flashtube (about 1 g). It was postulated that this was a reasonable amount of material ejected as combustion products from the mortar flashtube.

Computed wall pressures as a function of time for three locations along the tube wall (see figure 12) are displayed in figure 13. This figure can be used as a guide to the subsequent discussion of detailed modeling results displayed in figures 14–22. (Note that figures 14–22 have the ordinate magnified by about a factor of 7.) Prior to about 2.4 ms, propellant burning is confined to the tailboom, as evidenced by the nonexistent pressurization of the launch tube before this time. Early time pressure transients from about 2.6 to 2.75 ms indicate the bursting of the propellant increments. Pressure waves traveling between the rear and forward pressure taps are clearly evidenced by the alternating pressure peaks and troughs from about 3 to 4 ms. Subsequently, the launch tube is evenly pressurized, leading to projectile movement after about 5 ms. Essentially, the results of figure 13 are nearly identical to those of figure 3, with the obvious time shift of about 1.5 ms. This result indicates that the initiation of the centercore igniter in the mortar is less prompt than originally incorporated into the igniter table for region 1 but certainly just as energetic.

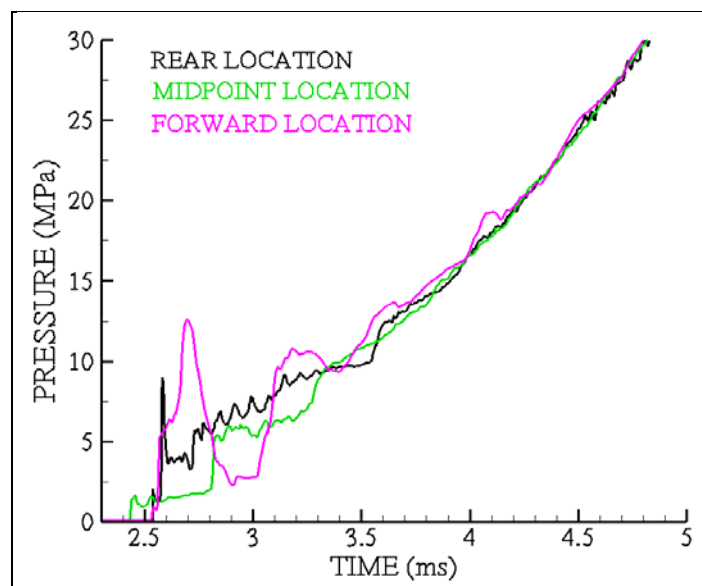


Figure 13. ARL-NGEN3 code results for tube wall pressures at three axial locations (see figure 12).

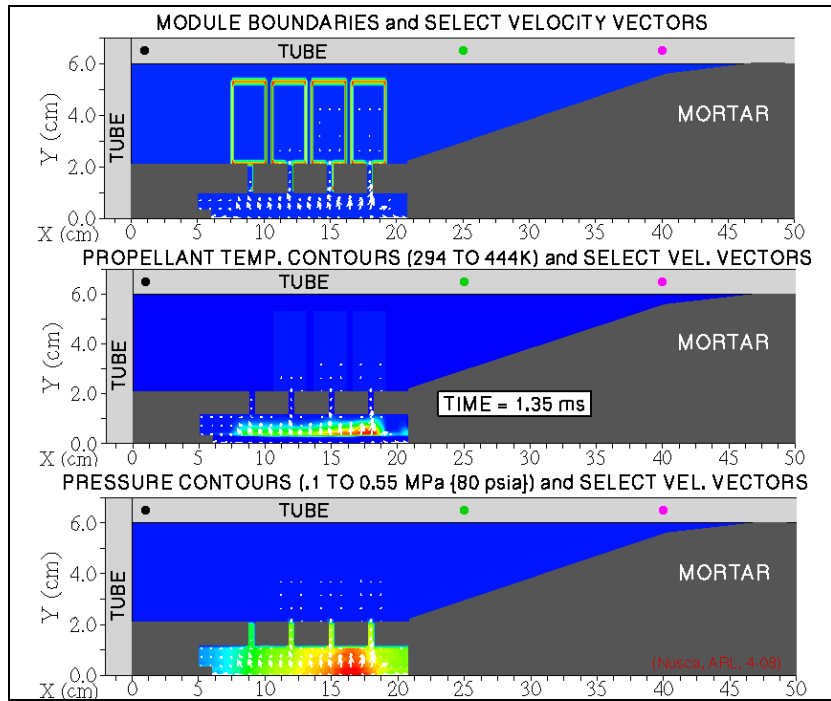


Figure 14. ARL-NGEN3 code results for contours of charge boundaries, propellant temperature, and gas pressure with selected velocity vectors. Time since igniter function is 1.35 ms.

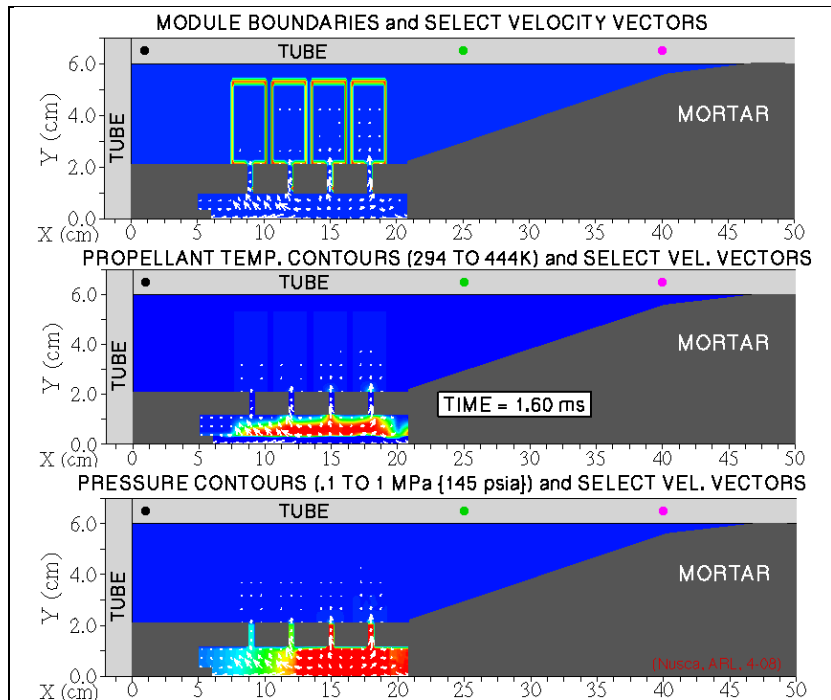


Figure 15. ARL-NGEN3 code results for contours of charge boundaries, propellant temperature, and gas pressure with selected velocity vectors. Time since igniter function is 1.6 ms.

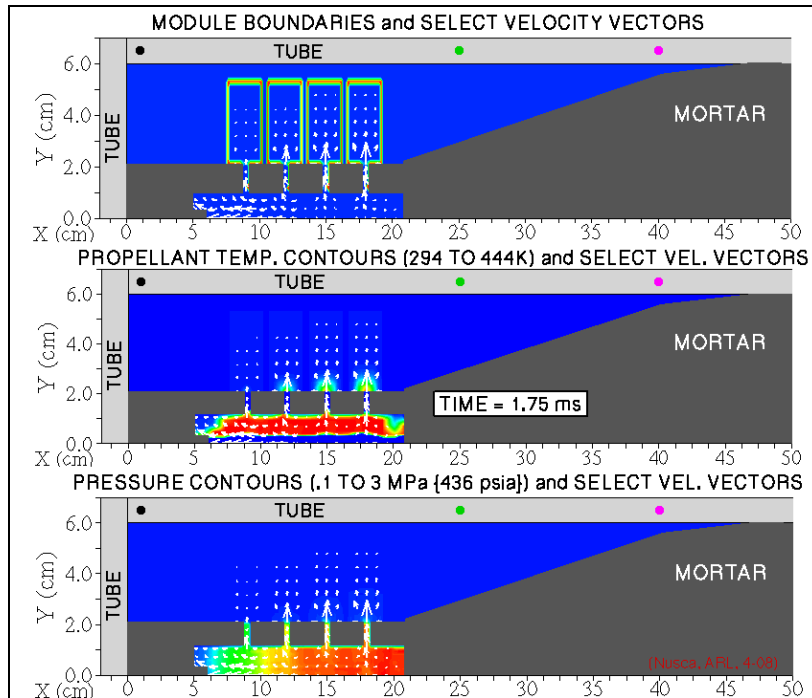


Figure 16. ARL-NGEN3 code results for contours of charge boundaries, propellant temperature, and gas pressure with selected velocity vectors. Time since igniter function is 1.75 ms.

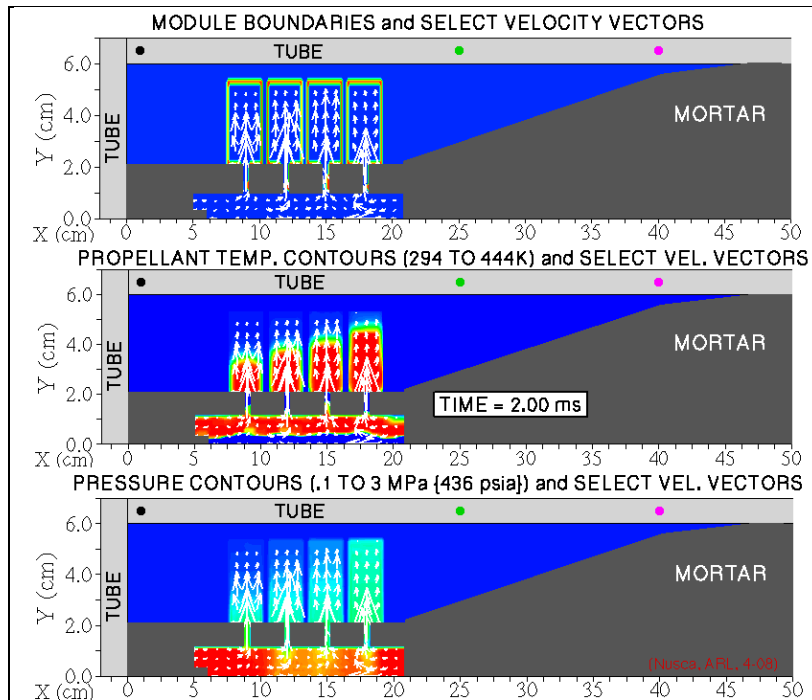


Figure 17. ARL-NGEN3 code results for contours of charge boundaries, propellant temperature, and gas pressure with selected velocity vectors. Time since igniter function is 2.0 ms.

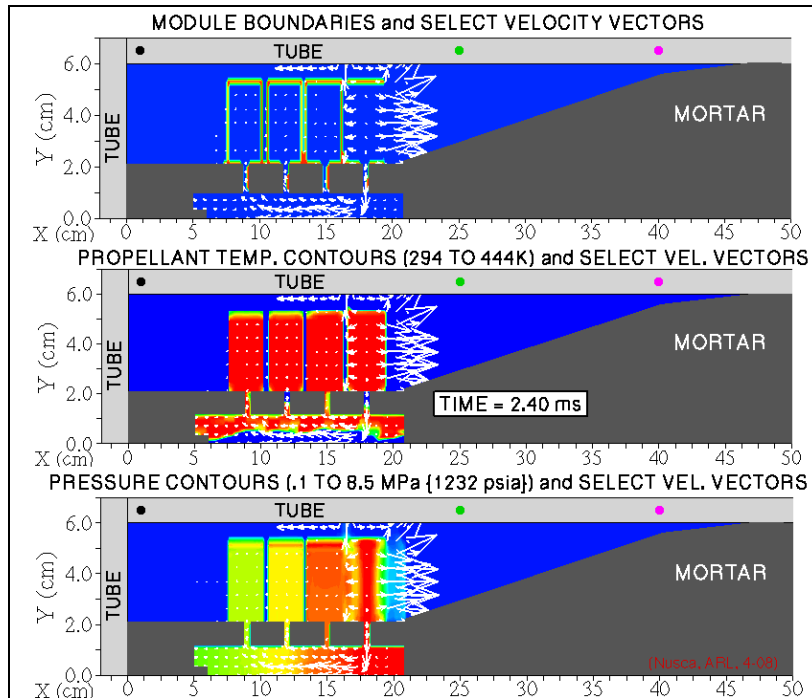


Figure 18. ARL-NGEN3 code results for contours of charge boundaries, propellant temperature, and gas pressure with selected velocity vectors. Time since igniter function is 2.4 ms.

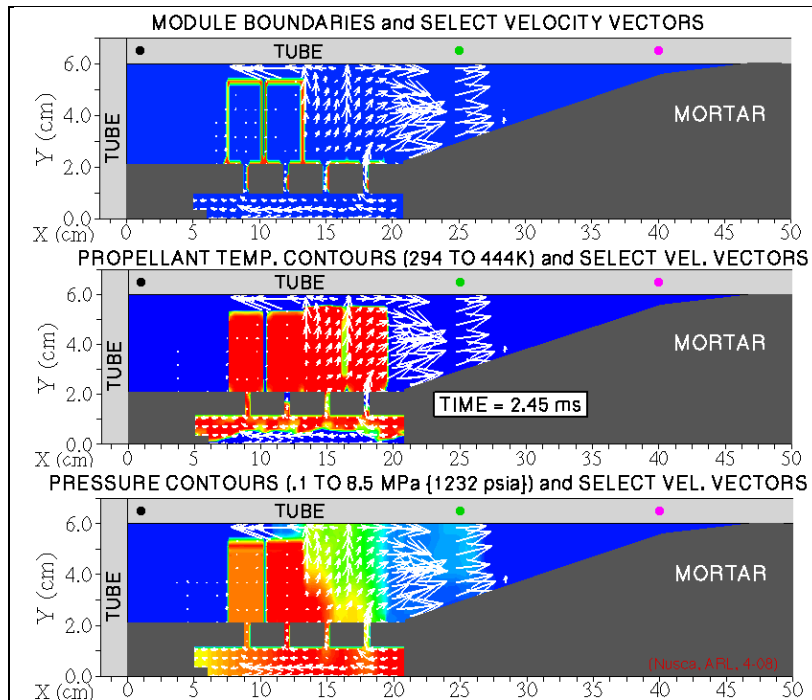


Figure 19. ARL-NGEN3 code results for contours of charge boundaries, propellant temperature, and gas pressure with selected velocity vectors. Time since igniter function is 2.45 ms.

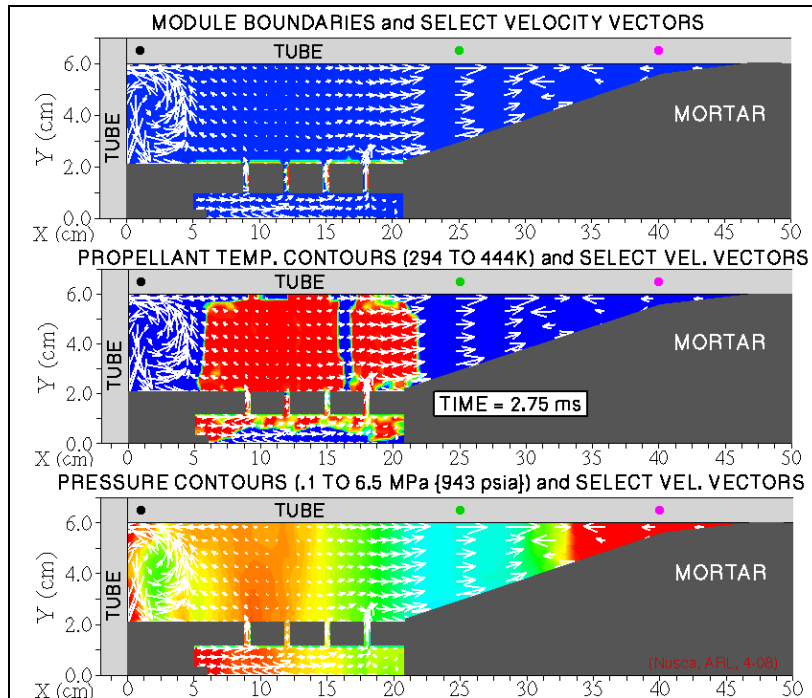


Figure 20. ARL-NGEN3 code results for contours of charge boundaries, propellant temperature, and gas pressure with selected velocity vectors. Time since igniter function is 2.75 ms.

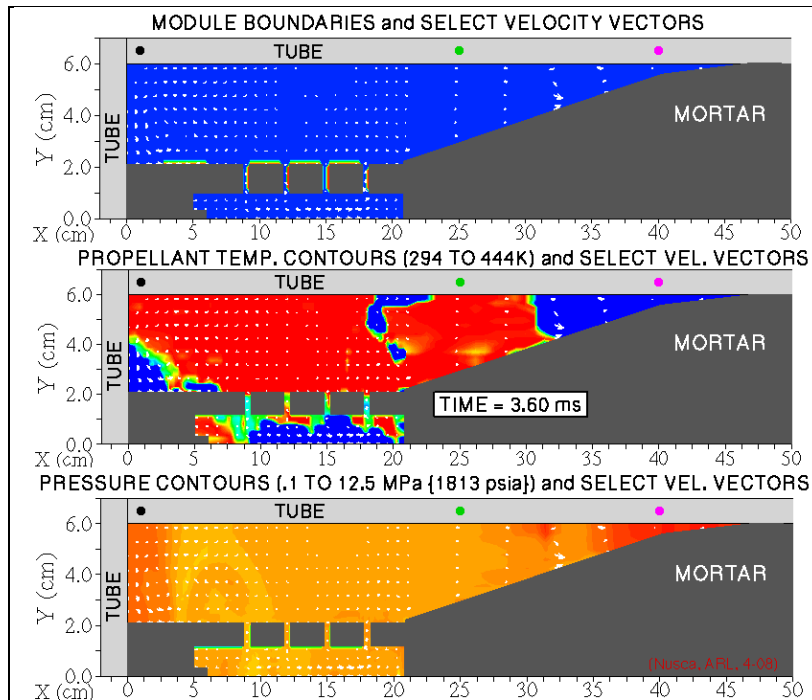


Figure 21. ARL-NGEN3 code results for contours of charge boundaries, propellant temperature, and gas pressure with selected velocity vectors. Time since igniter function is 3.6 ms.

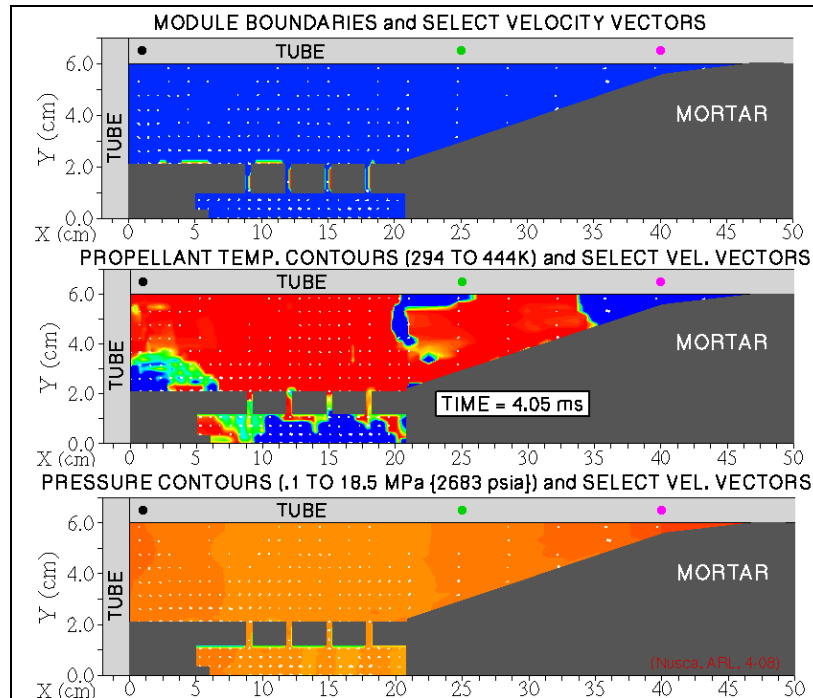


Figure 22. ARL-NGEN3 code results for contours of charge boundaries, propellant temperature, and gas pressure with selected velocity vectors. Time since igniter function is 4.05 ms.

The detailed results of the ARL-NGEN3 simulation are displayed in figures 14–22 for times of 1.35–4.05 ms from the start of outflow from region 1 (see figure 12). During this time period, the ignition and flame spreading are prominent, and it is after 5 ms that the mortar begins to travel down the tube (for brevity, modeling results are not presented for times greater than 4.05 ms). In each figure, a particular time is displayed using three computed variables—module boundaries, propellant temperature, and gas pressure. Velocity vectors (in white) are overlaid in each case that displays the magnitude (via vector length) and direction of the local gas field. Module boundaries are red when solid and change color to indicate loss in integrity due to a combination of burn-through and burst due to overpressure. When a charge module has fully disintegrated, module boundaries are no longer displayed. The location of ignited propellant is indicated from green to red (i.e., warm temperature to ignition temperature). High gas pressure is indicated by red, with lower pressures indicated by a succession of colors from orange to blue.

Figures 14 and 15 show results just past the start of the simulation. Burning BP within the inner igniter region 1 produces gases that flow radially and begin ignition of the M48 propellant within the tailboom. (Note that M48 at the axial extreme of this region initiates first due to the forward-biased gas generation built into the centercore igniter [i.e., as a direct result of the experimental data used to construct the igniter table for region 1]). Gases begin to flow into the annular slots, and flow stagnation to about 1 MPa is observed in the igniter. By 1.75 ms (figure 16), the M48

propellant is fully ignited and pressurization of the enclosed tailboom is about 3 MPa. Even though the increments are still intact, high-pressure flow through the annular slots in the tailboom has begun to penetrate the four propellant modules external to the tailboom. By 2.0 ms (figure 17), high-velocity gas flow through the annular slots and into the increments has caused ignition of the still-contained M47 propellant. As expected, the fourth increment (i.e., region 6) shows advanced flame spreading owed to the higher pressure (stagnated) gas in the forward end of the tailboom. Subsequently, by 2.4 ms (figure 18), the fourth increment bursts due to overpressures exceeding 8.5 MPa. Due to the support provided by the third increment, the burst of the fourth increment occurs in the forward direction. In response to the burst event, the rearward movement of the remaining intact increments has closed the interincrement gaps.

It is interesting to note the gas flow is now forced back down through the fourth annular slot and into the tailboom, raising the internal pressure to about 8.5 MPa, while M48 propellant within the tailboom is forced up through the first and second annular slots. By 2.45 ms (figure 19), another increment yields, and by 2.75 ms (figure 20), all of the increments have been burst and M47 propellant is free to move in the launch tube. Whereas, high pressure in the launch tube had been confined to the region near the propellant increments, uneven pressurization of the entire launch tube behind the mortar after 2.75 ms (figure 21) is observed as well as several 2-D flow phenomena (e.g., vortices). One can also observe high-velocity gas flowing onto the mortar afterbody and returning to the rear of the launch tube. These pressure waves are the source of uneven forces and stresses on the mortar prior to launch. Between 3.6 and 4.05 ms (figures 21 and 22), unconfined M47 propellant is spreading throughout the launch tube as, essentially, even pressurization of the chamber to levels exceeding 18 MPa is occurring. After these events, the projectile begins forward motion up the launch tube. Reviewing figures 14–22 and paying special attention to the interior of the mortar tailboom, one can note a series of pressure waves that travel within this tube that are generated purely by gas flow and observed by Kuo et al. (2).

These detailed modeling results represent the first look at the ignition, flame spreading, and increment burst events for the 120-mm mortar. While it is clear that much has been achieved, the improved fidelity of the igniter tube within innermost regions of the tailboom remains to be completed. Since this region contains the primer, five BP pellets, and a perforated tube (i.e., all beneath the region of M48 propellant—recall figure 12, region 2), detailed modeling is relegated to a dedicated igniter submodel that is described in the next section and linked to the ARL-NGEN3 code.

3. Dedicated Igniter Submodel

Sections 2.1 and 2.2 show that the flame-spreading characteristics of the 120-mm mortar are directly dependent on the method used to represent the ignition stimulus, with a noted delay of 1.5 ms between the two examples shown previously. This delay is evidence that it is key to develop a submodel which captures as much of the relevant physics as possible. The goal of this section is to describe the development of said submodel, which includes a primer and five BP pellets. The model provides a variable diameter and density constant Reynolds number (Re) turbulent flow output, which is to be fed into the ARL-NGEN3 code.

The primer used in the 120-mm mortar is the Federal no. 150 (Fed 150). The exact formulation is proprietary to Federal, a wholly-owned subsidiary of ATK, Alliant Techsystems. The Fed 150 is a basic lead styphnate primer (13) similar to the no. 41 primer (a normal lead styphnate primer). In the absence of specific chemical makeup, the analysis given in Schmidt and Nusca (12) was considered sufficient. Table 1 provides the lead styphnate composition, and table 2 provides the thermochemical calculations done using Cheetah (14), the basis of which is discussed in Schmidt and Nusca (12). The Fed 150 primer is 1.54× larger in mass than the no. 41 primer, so the output of the Fed 150 primer is assumed to be a statistically-averaged, constant-mass generation rate lasting 1.54× as long as the no. 41 primer in this submodel at a bulk Re of 10,000, which is a turbulent Re of 356.

Table 1. Chemical composition of the no. 41 primer mixture.

| Name | Formula | Weight-Percent | ±Weight-Percent | Purpose |
|------------------|--|----------------|-----------------|-------------------|
| Lead styphnate | H ₃ C ₆ N ₃ O ₉ Pb | 37 | 5 | Primary explosive |
| Barium nitrate | Ba (N O ₃) ₂ | 32 | 5 | Oxidizer |
| Antimony sulfide | Sb ₂ S ₃ | 15 | 2 | Fuel |
| Aluminum powder | Al | 07 | 1 | Fuel |
| Tetracene | H ₈ C ₂ N ₁₀ O | 04 | 1 | Primary explosive |
| PETN | C ₅ H ₈ N ₄ O ₁₂ | 05 | 1 | High explosive |

Table 2. Cheetah code gun calculation results.

| Temperature (K) | Pressure (MPa) | Impetus (J/g) | Molecular Weight (g/g-mol) | Covolume (m ³ /g) | Gamma, Frozen |
|-----------------|----------------|---------------|----------------------------|------------------------------|---------------|
| 2797 | 7.4 | 530 | 44 | 0.635 | 1.176 |

Mean plug flow velocity (12) of 48.4 m/s is assumed. The fluid density $\rho = 0.12 \text{ g/cm}^3$, viscosity $= 8.17 \times 10^{-5} \text{ kg/m/s}$, and diameter $D = 0.0011938 \text{ m}$, which gives a bulk Re about 10,000. Assumed primer no. 41 conditions only changed the diameter of the hole to that of the

hole in the BP. The 1-D turbulence model (ODT) can compute instantaneous velocity profiles, representing all relevant turbulent velocity scales for the given Re.

The submodel output to the ARL-NGEN3 code consists of the mixing of the Fed 150 primer output discussed previously and the burning of the BP pellet. The BP burning rate is taken from Sasse (15) as $r = 1.72 p^{0.164}$, with the regression rate, r , in centimeter/second, and pressure, p , in atmospheres. Given the burning rate and initial geometries, standard ballistics models can be used to predict the change in geometry (e.g., the surface area) and the mass production rate of gas. The next step is to correctly model the primer output and the gas generated by burning BP in order to predict a variable density turbulent efflux into region 1 of figure 2.

To model the mixing of the primer output with the product of the BP, the macroscopic balances for nonisothermal flow systems are needed for mass, momentum, and energy, as shown in the following (equations 1, 2, and 3, respectively):

$$\frac{dm_{tot}}{dt} = -\Delta w, \quad (1)$$

$$\frac{d\tilde{P}_{tot}}{dt} = -\Delta \left(\frac{\langle v^2 \rangle}{\langle v \rangle} \tilde{w} + p\tilde{S} \right) - \tilde{F} + m_{tot} \tilde{g}, \quad (2)$$

and

$$\frac{d(U_{tot} + K_{tot} + \Phi_{tot})}{dt} = -\Delta \left[\left(\hat{U} + p\hat{V} + \frac{1}{2} \frac{\langle v^3 \rangle}{\langle v \rangle} + \Phi \right) w \right] + Q - W, \quad (3)$$

where

$$w \equiv \rho \langle \bar{v} \rangle S, \quad (4)$$

and m_{tot} is the total mass, w is the mass flow rate, P_{tot} is the total momentum of the system, \sim signifies a vector, $\langle v \rangle$ the time smoothed velocity, F the net force of the solid surfaces on the fluid, g is the gravitational acceleration, U is the internal energy, K is the internal kinetic energy, Φ is the potential energy, $\hat{\quad}$ signifies per unit mass, p is the pressure, V is the volume, Q is the heat input, W is the work done by the system, ρ is density, S is the surface area of the input and output streams (assumed perpendicular to the mean flow), and Δ is defined as the exit value minus the entrance values.

Assuming pseudo-steady-state, the equations are simplified as follows:

$$\Delta w = 0, \quad (5)$$

$$\tilde{F} = -\Delta \left(\frac{\langle v^2 \rangle}{\langle v \rangle} \tilde{w} + p\tilde{S} \right) + m_{tot} \tilde{g} , \quad (6)$$

and

$$\Delta \left[\left(\hat{U} + p\hat{V} + \frac{1}{2} \frac{\langle v^3 \rangle}{\langle v \rangle} + \Phi \right) w \right] = Q - W . \quad (7)$$

A reasonable assumption for turbulent flow is a nearly flat velocity profile across the channel, allowing the simplification of the $\langle v \rangle$ terms in equations 6 and 7. The Froude number, Fr , is of order 10, so the gravitational force can be neglected. No external force, F , negligible change in the potential energy Φ between the input and output streams, and work, W , done by the system exist. The pseudo-steady-state assumption is consistent, assuming that there is no net heat transfer, Q . Substituting H for $U + pV$, we get the simplified equations for mass, momentum, and energy as follows:

$$\Delta w = 0 , \quad (8)$$

$$\Delta (\langle v \rangle \tilde{w} + p\tilde{S}) = 0 , \quad (9)$$

and

$$\Delta \left[\left(\hat{H} + \frac{1}{2} \langle v^2 \rangle \right) w \right] = 0 . \quad (10)$$

Using the conservation of mass (equation 8) with the pseudo-steady-state assumption, the discretized density can be shown as follows:

$$\rho_i = \frac{m_{i-1} + m_p + m_{bi}}{V_{ci}} , \quad (11)$$

and

$$\rho_0 = \frac{m_p}{V_0} , \quad (12)$$

where the i is the current step and V_c is the volume channel in the BP pellets. The term m_p indicates mass from the primer. The term m_{bi} indicates the mass generated from the BP in this step, and the term m_{i-1} is the total mass in the system at the last time step. The initial condition (equation 12) states that the density of the gas in the system is the density of the generated primer gas before the BP pellets start to burn.

Utilizing the momentum and energy equations, along with the assumption of change in enthalpy, is given by the following:

$$\Delta H = \int_{T_1}^{T_2} \hat{C}_p dT, \quad (13)$$

where T is temperature, C_p is heat capacity at constant pressure, state T_1 is the temperature before mixing, and state T_2 is the temperature after mixing. It can be shown that the temperature of the mixture passed to the ARL-NGEN3 code in region 1 is given by the following:

$$T_2 = \frac{T_{pr} \hat{C}_p^{pr} + T_{BP} \hat{C}_p^{BP} + 1/2(\langle v_1^2 \rangle - \langle v_2^2 \rangle)}{\hat{C}_p^{pr} + \hat{C}_p^{BP}}. \quad (14)$$

The constant Re ODT velocity profile, along with the instantaneous density (equation 11) and the instantaneous temperature (equation 14), provides all the needed inputs for the ARL-NGEN3 code. The complete coupling of these models is the subject of future work.

4. Conclusions

Application of the 2-D ARL-NGEN3 model to mortars (i.e., ignoring the mortar tail fins for the present) using an explicit treatment of the solid propellant components and a conventional gas-phase igniter has demonstrated key points for the physics of a mortar system. Regions of reverse flow, nonsequential flame spreading, and module burst, as well as the generation of a reverse pressure gradient (i.e., high pressure onto the tail boom), were among the many new phenomena revealed using this code. The application of the conventional gas-phase igniter table was shown in figures 4–11. Key points of interest were demonstrated in accordance with expectations. An improved gas generation table designed to mimic the experimental measurements from an actual primer tube was utilized; the results shown in figures 14–22 demonstrate the expected flame-spreading phenomena with an ~1.5-ms lag. In the IB of mortars, a 1.5-ms time lapse may be critical. As such, an ambiguous 1.5-ms time difference prompted the development of a detailed mortar primer submodel for the ARL-NGEN3 code that will replace both the conventional gas generation table and a more accurate table, which was designed around experimental measurements. This new mortar/primer submodel was developed and should provide an adequate description of all the relevant physics that occur in the early part of the ignition phase of the mortar primer and the burning of the five BP pellets. This new submodel is to be coupled to the ARL-NGEN3 code as future work in mortar modeling.

5. References

1. Anderson, R. D. *IBHVG2: Mortar Simulation with Interior Propellant Canister*; ARL-TR-3760; U.S. Army Research Laboratory: Aberdeen Proving Ground, MD, March 2006.
2. Kuo, K.; Acharya, R.; Ferrara, P.; Moore, J. Method of Characteristics Simulation of Interior Ballistics Processes of M1020 Ignition Cartridge in a 120-mm Mortar System. *Proceedings of the 40th JANNAF Combustion Meeting*, Charleston, SC, 13–16 June 2005.
3. May, I. W.; Horst, A. W. Charge Design Considerations and their Effect on Pressure Waves in Guns. *Interior Ballistics of Guns (Progress in Astronautics and Aeronautics)*; Krier, H., Summerfield, M., Eds.; AIAA: New York, NY, 1979; Vol. 66.
4. Schmidt, J. R.; Nusca, M. J.; Horst, A. W. Mortar Interior Ballistics: Sensitivity Studies Using IBHVG2 and Progress Toward a Multi-Dimensional Representation. *Proceedings of the 54th JANNAF Propulsion Meeting*, Denver, CO, 14–17 May 2007.
5. Gough, P. S. Modeling Arbitrarily Packaged Multi-Increment Solid Propellant Charges of Various Propellant Configurations. *Proceedings of the 33rd JANNAF Combustion Meeting*; CPIA Publication 653, 1, 1996, pp 421–435.
6. Gough, P. S. *Extensions to the NGEN Code: Propellant Rheology and Container Properties*; CPIA Publication 662, 3, 1997, pp 265–281.
7. Nusca, M. J.; Gough, P. S. Numerical Model of Multiphase Flows Applied to Solid Propellant Combustion in Gun Systems, AIAA Paper No. 1998-3695. *Proceedings of the 34th Joint Propulsion Conference and Exhibit*, AIAA: Cleveland, OH, July 1998.
8. Nusca, M. J. *High-Performance Computing and Simulation for Advanced Armament Propulsion*; ARL-TR-3215; U.S. Army Research Laboratory: Aberdeen Proving Ground, MD, June 2004.
9. Nusca, M. J. *Numerical Simulation of the Interior Ballistics for the 105MM HEP-T M393A3*; U.S. Army Research Laboratory: Aberdeen Proving Ground, MD, in press, March 2008.
10. Nusca, M. J.; Horst, A. W. *Progress in Modeling Ignition in a Solid Propellant Charge for Telescoped Ammunition*; ARL-TR-3673; U.S. Army Research Laboratory: Aberdeen Proving Ground, MD, November 2005.

11. Horst, A. W.; Nusca, M. J. *The Charge Designer's Workbench: A Range of Interior Ballistic Modeling Tools*; ARL-TR-3796; U.S. Army Research Laboratory: Aberdeen Proving Ground, MD, May 2006.
12. Schmidt, J. R.; Nusca, M. J. *Progress in the Development of a Multiphase Turbulent Model of the Gas/Particle Flow in a Small Caliber Ammunition Primer*; ARL-TR-3860; U.S. Army Research Laboratory: Aberdeen Proving Ground, MD, August 2006.
13. Rempfer, E. U.S. Army Research Laboratory. Personal communication, 15 April 2008.
14. Fried, L. E.; Glaesemann, K. R.; Howard, W. M.; Souers, P. C.; Vitello, P. A. Cheetah Code, Version 4.0, UCRL-CODE-155944; Lawrence Livermore National Laboratory: Livermore, CA, 2005.
15. Sasse, R. A. *Strand Burn Rates of Black Powder to One Hundred Atmospheres*; BRL-TR-02490; U.S. Army Ballistics Research Laboratory: Aberdeen Proving Ground, MD, May 1983.

NO. OF
COPIES ORGANIZATION

1 DEFENSE TECHNICAL
(PDF INFORMATION CTR
only) DTIC OCA
8725 JOHN J KINGMAN RD
STE 0944
FORT BELVOIR VA 22060-6218

1 DIRECTOR
US ARMY RESEARCH LAB
IMNE ALC HRR
2800 POWDER MILL RD
ADELPHI MD 20783-1197

1 DIRECTOR
US ARMY RESEARCH LAB
AMSRD ARL CI OK TL
2800 POWDER MILL RD
ADELPHI MD 20783-1197

1 DIRECTOR
US ARMY RESEARCH LAB
AMSRD ARL CI OK PE
2800 POWDER MILL RD
ADELPHI MD 20783-1197

ABERDEEN PROVING GROUND

1 DIR USARL
AMSRD ARL CI OK TP (BLDG 4600)

| <u>NO. OF</u> <u>COPIES</u> | <u>ORGANIZATION</u> |
|--------------------------------|--|
| 3 | DIRECTOR US ARMY RESEARCH LAB AMSRD ARL RO P D MANN R ANTHENIEN TECH LIB PO BOX 12211 RESEARCH TRIANGLE PARK NC 27709-2211 |
| 8 | US ARMY AVIATN & MIS CMND AMSRD AMR PS PT W CHEW C DOLBEER J LILLY M LYON J FISHER B MARSH R MICHAELS D THOMPSON REDSTONE ARSENAL AL 35898-5249 |
| 1 | PM MAS SFAE AMO MAS M BUTLER BLDG 354 PICATINNY ARSENAL NJ 07806-5000 |
| 1 | PM CAS SFAE AMO CAS J RUTKOWSKI BLDG 171M PICATINNY ARSENAL NJ 07806-5000 |
| 8 | DIR BENET WEAPONS LAB M AUDINO R DILLON R FISCELLA R HASENBEIN E KATHE K MINER S SOPOK J MCNEIL WATERVLIET NY 12189-4000 |
| 1 | CDR US ARMY ARDEC R CARR BLDG 65N PICATINNY ARSENAL NJ 07806-5000 |

| <u>NO. OF</u> <u>COPIES</u> | <u>ORGANIZATION</u> |
|--------------------------------|---|
| 6 | CDR US ARMY ARDEC C ADAM P HUI S EINSTEIN J O'REILLY J SHIN E CARAVACA BLDG 382 PICATINNY ARSENAL NJ 07806-5000 |
| 1 | CDR US ARMY ARDEC R CIRINCIONE BLDG 171M PICATINNY ARSENAL NJ 07806-5000 |
| 2 | CDR US ARMY ARDEC J LANNON B MACHAK BLDG 1 PICATINNY ARSENAL NJ 07806-5000 |
| 1 | CDR US ARMY ARDEC E LOGSDEN BLDG 65S PICATINNY ARSENAL NJ 07806-5000 |
| 2 | CDR US ARMY ARDEC S NICHOLICH R SURAPANENI BLDG 3022 PICATINNY ARSENAL NJ 07806-5000 |
| 1 | CDR US ARMY ARDEC P O'REILLY BLDG 407 PICATINNY ARSENAL NJ 07806-5000 |
| 1 | CDR US ARMY ARDEC A SABASTO BLDG 94 PICATINNY ARSENAL NJ 07806-5000 |
| 1 | CDR RADFORD ARMY AMMO PLANT SMCAR QA HI LIB RADFORD VA 24141-0298 |
| 2 | CDR NAVAL RSRCH LAB TECH LIB J BORIS WASHINGTON DC 20375-5000 |

NO. OF
COPIES ORGANIZATION

4 OFFICE OF NVL RSRCH
J GOLDWASSER
D SIMONS
D ROBERSON
P COLOLLY
875 N RANDOLPH ST RM 653
ARLINGTON VA 22203-1927

1 CDR NSWC
TECH LIB
DAHLGREN VA 22448-5000

3 CDR NAWC
A ATWOOD
S BLASHILL
T PARR
CHINA LAKE CA 93555-6001

1 AIR FORCE RSRCH LAB
MNME EN MAT BR
B WILSON
2306 PERIMETER RD
EGLIN AFB FL 32542-5910

1 AIR FORCE OFC OF SCI RSRCH
M BERMAN
875 N RANDOLPH ST
STE 235 RM 3112
ARLINGTON VA 22203-1768

1 NASA LANGLEY RSRCH CTR
D BUSHNELL
MS 110
HAMPTON VA 23681-2199

1 DIR SANDIA NATL LABS
M BAER
DEPT 1512
PO BOX 5800
ALBUQUERQUE NM 87185

2 DIR LLNL
L FRIED
M MURPHY
PO BOX 808
LIVERMORE CA 94550-0622

1 CENTRAL INTLLGNC AGCY
J BACKOFEN
RM 4PO7 NHB
WASHINGTON DC 20505

NO. OF
COPIES ORGANIZATION

1 BATTELLE EAST SCI & TECH
A ELLIS
1204 TECHLGY DR
ABERDEEN MD 21001-1228

2 JHU CHEM PROP INFO AGCY
W HUFFERD
R FRY
10630 LITTLE PATUXENT PKWY
STE 202
COLUMBIA MD 21044-3200

1 (CD
only) OUSD (AT&L)/STRAT & TACT
SYS MUNITIONS
T MELITA
3090 DEFENSE PENTAGON
RM 3B1060
WASHINGTON DC 20301-3090

1 BRIGHAM YOUNG UNIV
DEPT OF CHEM ENGRG
M BECKSTEAD
PROVO UT 84601

1 CALIF INST OF TECHLGY
F CULICK
204 KARMAN LAB
MS 301 46
1201 E CALIFORNIA ST
PASADENA CA 91109

2 UNIV OF ILLINOIS
DEPT OF MECH INDUST
ENGRNG
H KRIER
R BEDDINI
144 MEB 1206 N GREEN ST
URBANA IL 61801-2978

5 PENN STATE UNIV
DEPT OF MECHL ENGRG
K KUO
T LITZINGER
G SETTLES
S THYNELL
V YANG
UNIVERSITY PARK PA 16802-7501

1 INST FOR ADVNCD TECHN LGY
3925 W BRAKER LN STE 400
AUSTIN TX 78759-5316

NO. OF
COPIES ORGANIZATION

1 ARROW TECHLGY ASSOC INC
1233 SHELBURNE RD D 8
SOUTH BURLINGTON VT 05403

1 ALLEGHENY BALLISTICS LAB
PO BOX 210
ROCKET CENTER WV 26726

1 ATK ORDNANCE
4700 NATHAN LANE
PLYMOUTH MN 55442

3 ATK AMMO & ENERGETICS
RADFORD ARMY AMMO PLANT
D WORRELL
W WORRELL
S RITCHIE
RT 114 PO BOX 1
RADFORD VA 24141-0299

4 ATK THIOKOL
P BRAITHWAITE
T FARABAUGH
W WALKUP
R WARDLE
PO BOX 707
BRIGHAM CITY UT 84302-0707

1 ATK ELKTON
J HARTWELL
PO BOX 241
ELKTON MD 21921-0241

1 BAE ARMAMENT SYS DIV
J DYVIK
4800 E RIVER RD
MINNEAPOLIS MN 55421-1498

1 GEN DYNAMICS ST MARKS
H RAINES
PO BOX 222
SAINT MARKS FL 32355-0222

1 GEN DYNAMICS ARM SYS
J TALLEY
128 LAKESIDE AVE
BURLINGTON VT 05401

3 VERITAY TECHGY INC
R SALIZONI
J BARNES
E FISHER
4845 MILLERSPORT HWY
EAST AMHERST NY 14501-0305

NO. OF
COPIES ORGANIZATION

2 DIRECTOR
US ARMY RSRCH LAB
IMNE ALC PWO
G BROWN
2800 POWDER MILL RD
ADELPHI MD 20783-1197

ABERDEEN PROVING GROUND

55 DIR USARL
AMSRD ARL WM
B FORCH
P PLOSTINS
AMSRD ARL WM B
M ZOLTOSKI
AMSRD ARL WM BD
W ANDERSON
R BEYER
A BRANT
S BUNTE
C CANDLAND
L CHANG
J COLBURN
P CONROY
B HOMAN
A HORST
S HOWARD
P KASTE
A KOTLAR
R LIEB
K MCNESBY
M MCQUAID
A MIZIOLEK
J MORRIS
J NEWILL
M NUSCA (5 CPS)
R PESCE-RODRIGUEZ
S PIRAINO
B RICE
R SAUSA
E SCHMIDT
J SCHMIDT (4 CPS)
A WILLIAMS
AMSRD ARL WM BA
B DAVIS
D HEPNER (3 CPS)
G KATULKA
D LYON
AMSRD ARL WM BC
G COOPER
J DESPIRITO
F FRESCONI
J GARNER

NO. OF
COPIES ORGANIZATION

B GUIDOS
J SAHU
S SILTON
P WEINACHT
AMSRD ARL WM M
S MCKNIGHT
AMSRD ARL WM SG
T ROSENBERGER
AMSRD ARL WM T
P BAKER
W CIEPIELA

INTENTIONALLY LEFT BLANK.